### Synthesis and high-temperature oxidation resistance of SiC-ZrB<sub>2</sub> composite powders via carbothermal reduction

Yu Cao<sup>a,b</sup>, Yueming Li<sup>a,\*</sup>, Kai Li<sup>a</sup>, Chuanming Zou<sup>a</sup>, Jilin Hu<sup>b</sup> and Jin Wen<sup>b</sup>

<sup>a</sup>School of Materials Science and Engineering, Jingdezhen Ceramic University, China National Light Industry Key Laboratory of Functional Ceramic Materials, Jingdezhen 333403, Jiangxi, China

SiC-ZrB<sub>2</sub> composite powders were synthesized via carbothermal reduction using silica sol (SiO<sub>2</sub>·nH<sub>2</sub>O), graphite (C), boric acid (H<sub>3</sub>BO<sub>3</sub>), and zirconium dioxide (ZrO<sub>2</sub>) as raw materials. The effect of calcination temperature on the synthesis process was investigated by holding the mixture at temperatures ranging from 1450 to 1600 °C for 1 h. Composite powders synthesized under optimized conditions was subsequently selected to systematically evaluate its high-temperature oxidation resistance. Results indicate that holding at 1600 °C for 1 h represents the optimal synthesis condition, producing high-purity SiC-ZrB<sub>2</sub> composite powders. The powder exhibits a heterogeneous microstructure comprising near-spherical particles, columnar particles, irregularly structured particles, and whiskers. Stepwise oxidation testing revealed the following: At 800 °C, ZrB<sub>2</sub> was completely oxidized to ZrO2, while a small amount of SiC reacted with oxidation products to form zircon (ZrSiO4). Above 1200 °C, the oxidation of SiC increased substantially, accompanied by significant sintering, leading to the formation of dense agglomerates. Notably, SiC remained stable at 1500 °C, exhibiting markedly superior oxidation resistance compared to ZrB<sub>2</sub>.

Keywords: Carbothermal reduction, SiC-ZrB<sub>2</sub>, Composite powders, Preparation, Oxidation resistance.

#### Introduction

Ultra-high temperature ceramic (UHTC) materials are characterized by their high melting points, exceptional hardness, strong chemical stability, and excellent thermal shock resistance. These properties, retained even in high-temperature environments, make them suitable for widespread applications in fields such as metallurgy, electronics, energy, cutting tools, and aerospace [1-5]. SiC-ZrB<sub>2</sub> composites synergize the outstanding properties of ZrB<sub>2</sub> and SiC, achieving complementary advantages. These composites exhibit superior oxidation/ ablation resistance, high-temperature durability, and erosion resistance, while also retaining good mechanical properties at both room and elevated temperatures [6-9]. Consequently, they hold significant promise for applications in severe thermo-chemical environments, including hypersonic vehicle components, rocket propulsion systems, and specialized melting crucibles [10].

Conventional methods for preparing SiC-ZrB<sub>2</sub> composites typically involve mechanical blending of pre-synthesized SiC and ZrB<sub>2</sub> powders. However, this approach often results in inhomogeneous composition

distribution within the mixed powders. Such inhomo-

geneity can lead to microstructural defects—including agglomeration and porosity—in the final sintered composites, significantly degrading their mechanical properties, thermal performance, and other critical characteristics. Consequently, synthesizing composite powders with fine particle size, high sintering activity, uniform mixing, and excellent dispersion is essential for fabricating SiC-ZrB2 composites with superior comprehensive properties.

Compared to mechanical mixing, chemical synthesis routes offer distinct advantages for producing ultrafine, homogeneous composite powders [11]. Current chemical methods for synthesizing SiC-ZrB<sub>2</sub> powders primarily include carbothermal reduction [12-14], sol-gel processing [15, 16], combustion synthesis [17], plasma spraying [18], and microwave synthesis [19, 20]. Among these, carbothermal reduction is widely adopted due to its simple process, low cost, controllable reaction parameters, and consistent product quality. For instance, Zhou et al. [13] investigated the effects of calcination temperature and raw material ratios on synthesizing ZrB2-SiC-LaB6 composite powders using zirconyl chloride octahydrate (ZrOCl<sub>2</sub>·8H<sub>2</sub>O), boric acid (H<sub>3</sub>BO<sub>3</sub>), lanthanum chloride heptahydrate (LaCl<sub>3</sub>·7H<sub>2</sub>O), tetraethyl orthosilicate (TEOS), and glucose ( $C_6H_{12}O_6$ ) as precursors. Similarly, Lian et al. [14] synthesized ZrB<sub>2</sub>-SiC composite powders containing in situ grown SiC whiskers via a molten-saltassisted iron-catalyzed carbothermal reduction method.

\*Corresponding author: Tel: +86 13767842606 E-mail: lym6329@163.com

<sup>&</sup>lt;sup>b</sup>School of Materials and Environmental Engineering, Hunan University of Humanities, Science and Technology, Hunan Provincial Key Laboratory of Fine Ceramics and Powder Materials, Loudi 417000, Hunan, China

They systematically investigated the effects of heating temperature and iron catalyst content on SiC whisker growth behavior within the powders. Furthermore, a molten-salt-assisted iron-catalyzed vapor-solid (VS) mechanism was proposed to elucidate the growth mechanism of these whiskers.

Currently, research on synthesizing SiC-ZrB2 composite powders via carbothermal reduction using silica sol (as the silicon source), ZrO<sub>2</sub> (as the zirconium source), and graphite (as the carbon source) is limited. Furthermore, while studies on the oxidation resistance of SiC-ZrB<sub>2</sub> materials predominantly focus on bulk ceramics or coatings, investigations into the oxidation behavior of the composite powders themselves are relatively scarce. This gap is significant because SiC-ZrB<sub>2</sub> composite powders, due to their high specific surface area and surface energy, are susceptible to premature oxidation at lower temperatures. In contrast, dense SiC-ZrB2 bulk materials exhibit a higher oxidation threshold, as oxygen diffusion is hindered by their consolidated microstructure. Consequently, understanding the oxidation resistance of the composite powders is crucial for guiding their safe storage, effective processing, and reliable application in extreme high-temperature environments. Such studies also provide essential insights into the differences in oxidation behavior between powder and bulk forms, aiding in revealing the underlying synergistic oxidation mechanisms between the SiC and ZrB<sub>2</sub> phases. To address these research gaps, SiC-ZrB2 composite powders was first synthesized via carbothermal reduction in a hightemperature tube furnace under argon atmosphere, with specific focus on the effect of calcination temperature (1450 °C, 1550 °C, and 1600 °C). Subsequently, the high-temperature oxidation resistance of the synthesized powder was systematically evaluated through stepwise testing at 800 °C, 1000 °C, 1200 °C, and 1500 °C.

#### **Materials and Methods**

#### **Experimental procedure**

Graphite (C, ≥99%, Sinopharm Chemical Reagent Co., Ltd.), silica sol (mSiO<sub>2</sub>·nH<sub>2</sub>O<sub>2</sub>, industrial grade, 27 wt% SiO2, Changsha Water Glass Factory), zirconium dioxide (ZrO<sub>2</sub>, ≥98.5%, Sinopharm Chemical Reagent Co., Ltd.), and boric acid (H<sub>3</sub>BO<sub>3</sub>, ≥99.0%, Xiangzhong Chemical Reagent Co., Ltd.) were used. Raw materials were formulated to target a SiC:ZrB2 molar ratio of 7:3 in the final composite. To ensure complete carbothermal reduction, graphite was added at 110% of the theoretical stoichiometric requirement (10 wt% excess). Due to potential boron loss from H<sub>3</sub>BO<sub>3</sub> volatilization during synthesis, H<sub>3</sub>BO<sub>3</sub> was added at 120% of theoretical value (20 wt% excess) to ensure adequate boron availability. Precisely weighed materials were transferred to a ball mill jar with an ethanol-water solution as the liquid medium and ZrO<sub>2</sub> milling balls (ball-to-powder ratio: 3:1). Planetary ball milling was performed at 400 rpm for 4 h. The resulting slurry was dried at 100 °C for 24 h in an electric blast oven, then ground using an agate mortar. The precursor mixture was calcined in a high-temperature tube furnace under high-purity Argon atmosphere. Samples were heated to target temperatures (1450 °C, 1550 °C, or 1600 °C) at 10 °C/min, held for 1 h, and furnace-cooled. Composite powders synthesized at 1600 °C was placed in a corundum crucible within a box furnace. Oxidation resistance was evaluated by exposing samples to air at 800 °C, 1000 °C, 1200 °C, and 1500 °C for 30 min.

#### Test analysis

The phase composition of as-synthesized powders (calcined under Argon at 1450-1600 °C) and oxidized products (after exposure to air at 800-1500 °C) was analyzed using X-ray diffraction (XRD, Y-2000A diffractometer). Powder microstructure was characterized using scanning electron microscopy (SEM, Zeiss Sigma 500) and transmission electron microscopy (TEM, FEI Talos F200S). Elemental composition and distribution within micro-regions were determined by energy-dispersive X-ray spectroscopy (EDX) coupled with the SEM and TEM instruments.

#### **Results and Discussion**

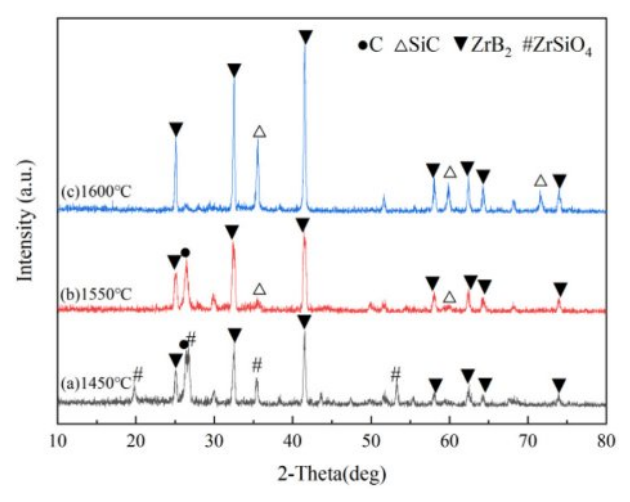
#### Phase composition of as-prepared composite powders

Fig. 1 presents the XRD patterns of powders synthesized under argon at 1450 °C, 1550 °C, and 1600 °C (1 h hold), demonstrating the significant influence of calcination temperature on phase composition. At 1450 °C, diffraction peaks correspond to residual carbon (C), intermediate zircon (ZrSiO<sub>4</sub>), and zirconium diboride (ZrB<sub>2</sub>), indicating partial reaction of ZrO<sub>2</sub> with SiO<sub>2</sub> forming ZrSiO<sub>4</sub> and with C yielding ZrB<sub>2</sub>. As temperature increased, ZrSiO<sub>4</sub> peak intensity gradually decreased and eventually disappeared by 1550 °C, signifying its decomposition, while ZrB<sub>2</sub> peak intensity concurrently increased. At 1550 °C, only strong C and ZrB2 peaks accompanied by weak silicon carbide (SiC) peaks were observed; the absence of ZrSiO<sub>4</sub> confirms its complete decomposition, while the presence of SiC signals the onset of carbothermal reduction between SiO2 and C. At 1600 °C, the pattern exclusively displays characteristic SiC and ZrB<sub>2</sub> peaks with no detectable impurities, confirming complete carbothermal reduction. These findings collectively demonstrate that a 1600 °C hold for 1 h enables full reaction progression, successfully yielding high-purity SiC-ZrB<sub>2</sub> composite powders.

It is noteworthy that in this experimental system, in addition to the  $ZrSiO_4$  intermediate phase mentioned earlier (which can be observed in the XRD pattern of Fig. 1), another type of intermediate phase may also form within the temperature range of 1000-1200 °C — specifically, the  $B_2O_3 \cdot SiO_2$  phase formed by the combination of  $B_2O_3$  and  $SiO_2$ . The formation

process of this intermediate phase can be divided into two steps: first, H<sub>3</sub>BO<sub>3</sub> in the raw materials starts to decompose at approximately 400 °C (reaction formula:  $H_3BO_3 \rightarrow B_2O_3 + H_2O\uparrow$ ), releasing  $B_2O_3$ ; subsequently, the generated B<sub>2</sub>O<sub>3</sub> undergoes a eutectic reaction with SiO<sub>2</sub> in the system at high temperature, forming a lowmelting-point B<sub>2</sub>O<sub>3</sub>·SiO<sub>2</sub> glass phase. As the reaction temperature further rises above 1300 °C, this glass phase will gradually react with ZrO2 in the system to generate ZrSiO<sub>4</sub>, while releasing B<sub>2</sub>O<sub>3</sub> vapor; the released B<sub>2</sub>O<sub>3</sub> vapor will continue to react with excess C to form B<sub>4</sub>C, and B<sub>4</sub>C will further react with ZrO<sub>2</sub> and C to generate ZrB<sub>2</sub>. When the temperature rises to 1600 °C, the entire series of intermediate phase transformation processes mentioned above are completed, ultimately forming pure SiC-ZrB<sub>2</sub> composite powders.

Furthermore, from the perspective of reaction mechanism, under high-temperature conditions, there is theoretically a possibility that graphite and ZrO<sub>2</sub> in the raw materials react to form the ZrC intermediate



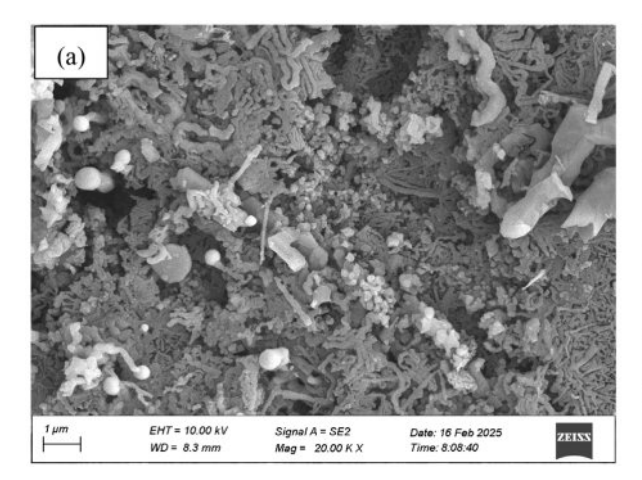
**Fig. 1.** XRD patterns of powders obtained by calcination at 1450 °C, 1550 °C, and 1600 °C for 1 h under argon.

phase. However, based on the XRD detection results of this experiment (Fig. 1), no clear diffraction peaks of other intermediate phases such as the  $B_2O_3\cdot SiO_2$  glass phase,  $B_4C$ , or ZrC were observed except for ZrSiO\_4. This phenomenon is mainly closely related to the experimentally set reaction thermodynamic conditions (temperature range of 1450–1600 °C) and raw material ratio (Si:Zr molar ratio of 7:3): under these conditions, the energy state of the reaction system tends to directly generate the two target products, SiC and ZrB\_2, thereby significantly reducing the probability of forming other intermediate phases.

In addition to the intermediate phases discussed above, from the perspective of thermodynamic calculation, boride intermediate phases such as ZrB4 and SiB6 may also theoretically exist in this reaction system. However, the presence of these phases was not detected in this experiment either, and the core reasons can be attributed to two aspects: first, in terms of thermodynamic stability, the formation free energy of ZrB4 and SiB6 is higher than that of ZrB<sub>2</sub> and SiC. According to the principle of minimum energy, the reaction tends to generate ZrB<sub>2</sub> and SiC, which have lower energy and higher stability; second, from the perspective of reaction kinetics, the parameters of the carbothermal reduction process set in this study (calcination temperature of 1600 °C and holding time of 1 h) are more suitable for the formation process of ZrB2 and SiC. In contrast, the formation of ZrB<sub>4</sub> and SiB<sub>6</sub> requires higher temperatures (usually exceeding 1800 °C) or longer holding times, which cannot be met by the existing experimental conditions. Therefore, such boride intermediate phases were not detected.

## Microscopic morphology of the as-prepared composite powders

Fig. 2 presents SEM micrographs of the composite powders synthesized at 1600 °C for 1 h under argon, revealing a heterogeneous microstructure comprising



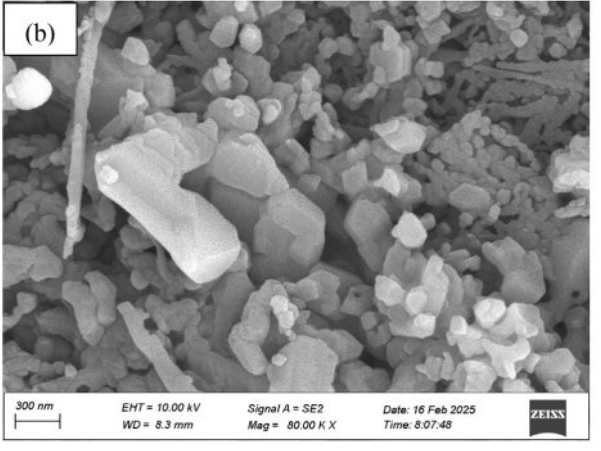


Fig. 2. SEM micrographs of the composite powders synthesized at 1600 °C for 1 h under argon. (a) Low magnification; (b) High magnification.

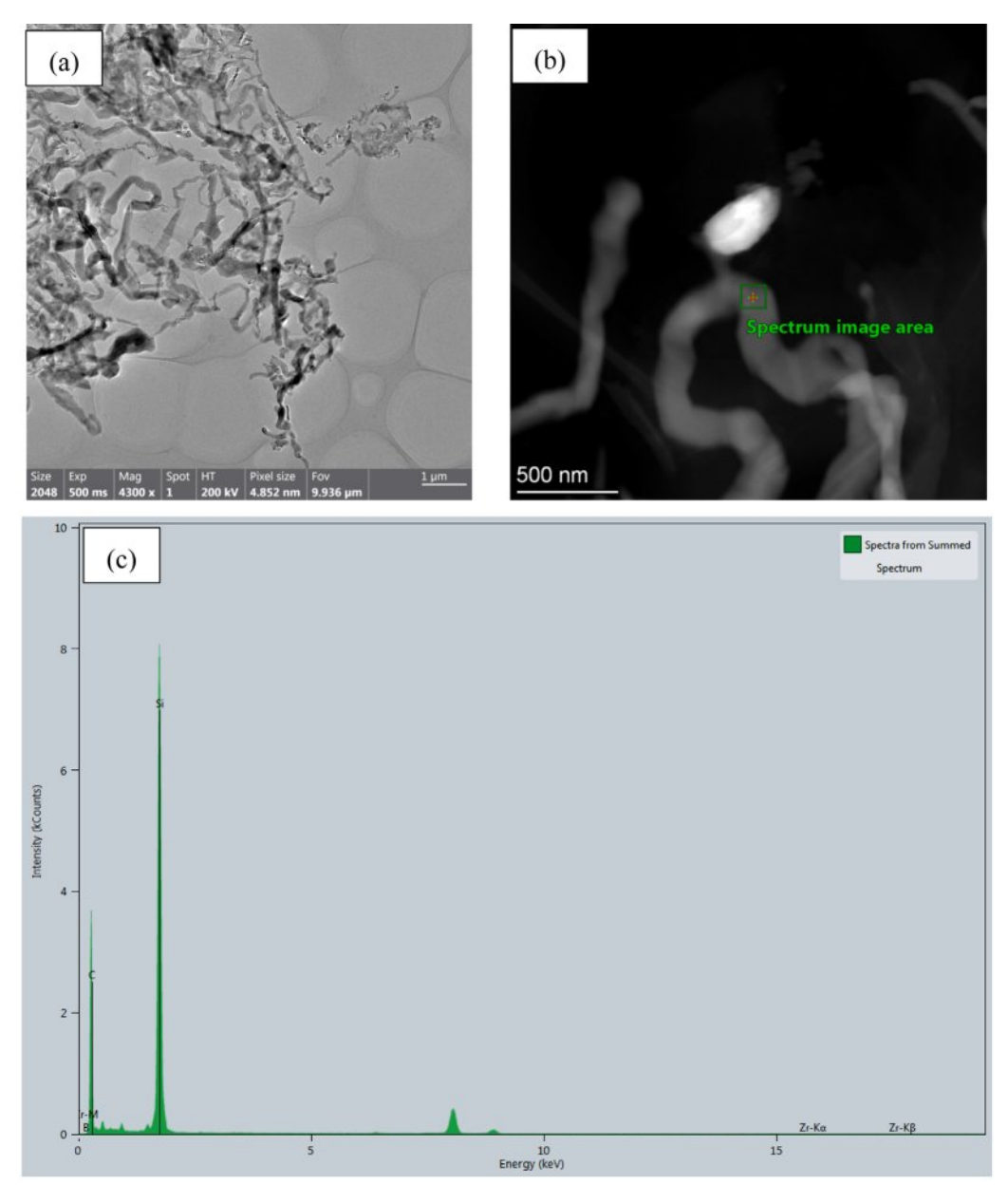


Fig. 3. TEM images and EDX analysis results of the composite powders synthesized at 1600 °C for 1 h under argon.

quasi-spherical particles (50–150 nm), columnar particles, irregular aggregates, and abundant whisker-like features (~50–100 nm diameter). Complementary TEM analysis (Fig. 3) further elucidates these whiskers as slender, curved structures exhibiting distinctive bamboo-joint morphology, often forming interconnected networks. Based on characteristic carbothermal reduction pathways [21-24] and concomitant EDX analysis (Fig. 3c), these whisker-like features are conclusively identified as silicon carbide (SiC).

# High-temperature oxidation resistance properties of the as-prepared composite powders

Fig. 4 presents XRD patterns of SiC-ZrB<sub>2</sub> composite powders oxidized at 800 °C, 1000 °C, 1200 °C, and

1500 °C (30 min). At 800 °C, diffraction peaks confirm complete oxidation of ZrB<sub>2</sub> to ZrO<sub>2</sub> (absence of ZrB<sub>2</sub> peaks), while residual SiC coexists with newly formed ZrSiO<sub>4</sub>—the latter resulting from partial reaction between oxidized SiC-derived SiO<sub>2</sub> and ZrO<sub>2</sub>. By 1000 °C, while phase composition remains qualitatively similar, intensified ZrO<sub>2</sub> peak intensities indicate progressive ZrB<sub>2</sub> oxidation. A significant transition occurs at 1200 °C: SiC peak intensities substantially diminish with concurrent ZrSiO<sub>4</sub> enhancement. At 1500 °C, despite persistent ZrSiO<sub>4</sub> formation, SiC maintains strong diffraction intensity. These results demonstrate SiC's superior oxidation resistance versus ZrB<sub>2</sub>, with SiC retaining structural stability even under 1500 °C oxidative extremes.

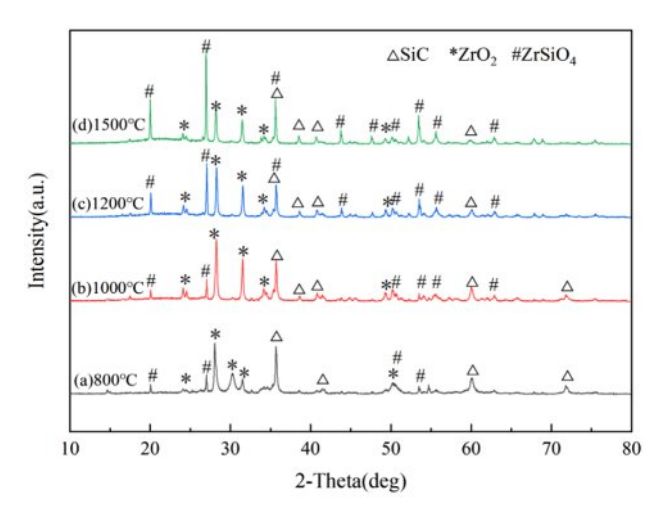


Fig. 4. XRD patterns of SiC-ZrB<sub>2</sub> composite powders oxidized at varied temperatures for 30 min.

Table 1 summarizes principal chemical reactions governing SiC-ZrB<sub>2</sub> composite powders oxidation in air. Oxidation behavior is governed by intrinsic factors (particle size, purity) and extrinsic parameters (heating rate, dwell time). Unlike bulk materials, the powder's

**Table 1.** Principal chemical reactions governing SiC-ZrB<sub>2</sub> composite powders oxidation in air [25-28].

NO.	Chemical reactions
(1)	$5ZrB_2(s) + 2O_2(g) = 5ZrO_2(s) + 5B_2O_3(l)$
(2)	$B_2O_3(l) = B_2O_3(g)$
(3)	$SiC(s)+2O_2(g) = SiO_2(s) + CO_2(g)$
(4)	$ZrO_2(s)+SiO_2(s) = ZrSiO_4(s)$
(5)	$xSiO_2(1) + yB_2O_3(g) = Si_xO_{2x}B_{2y}O_{3y}(1)$

**Table 2.** Mass change of SiC-ZrB<sub>2</sub> composite powders after oxidation treatment at different temperatures for 30 min.

Oxidation temperatures/°C	800	1000	1200	1500
Weight gain rate/%	20.2	23.9	16.3	10.5

high specific surface area dramatically increases oxygenaccessible reactive sites, accelerating oxidation kinetics. While ZrB<sub>2</sub> exhibits moderate oxidation resistance, powder oxidation initiates at 500–600 °C via Reaction (1), forming ZrO<sub>2</sub> and B<sub>2</sub>O<sub>3</sub>. Below 450 °C, viscous B<sub>2</sub>O<sub>3</sub> forms a protective surface layer; above 1000 °C,



**Fig. 5.** Macroscopic morphology of SiC-ZrB<sub>2</sub> composite powders after 30-min oxidation at: (a) 800 °C, (b) 1000 °C, (c) 1200 °C, (d) 1500 °C.

its volatility eliminates this protection, enabling rapid oxidation [25, 26]. SiC oxidation (Reaction 3) becomes significant at 800-1000 °C (lowered to 800 °C for nano/submicron powders due to enhanced reactivity). Initial SiO<sub>2</sub> formation creates a diffusion barrier [27, 28], though its protective efficacy is limited by: (1) inherent oxygen permeability even at 800 °C, and (2) cumulative oxidation across numerous particles exceeding bulk material degradation. Progressive heating to 1500 °C intensifies oxidation rates for both phases, with SiC demonstrating superior stability relative to ZrB<sub>2</sub>.

Table 2 summarizes mass changes in SiC-ZrB<sub>2</sub> composite powders oxidized at 800 °C, 1000 °C, 1200 °C, and 1500 °C (30 min). The weight gain rate exhibits a non-monotonic trend: increasing from 20.2% (800 °C) to a maximum 23.9% (1000 °C), then decreasing to 16.3% (1200 °C) and 10.5% (1500 °C). This behavior stems from competing mechanisms: oxidation reactions (Reactions 1 & 3) incorporate oxygen into solid products (ZrO<sub>2</sub>, SiO<sub>2</sub>, non-volatilized B<sub>2</sub>O<sub>3</sub>), increasing mass, while B<sub>2</sub>O<sub>3</sub> volatilization reduces mass. Below 1200 °C, minimal B<sub>2</sub>O<sub>3</sub> volatility allows oxygen incorporation to dominate, explaining the increasing weight gain up to 1000 °C. Above 1200 °C, accelerated B<sub>2</sub>O<sub>3</sub> volatilization outweighs oxygen incorporation from intensified oxidation, resulting in progressively lower net weight gain with temperature.

Fig. 5 documents the visual evolution of SiC-ZrB<sub>2</sub> composite powders oxidized at 800-1500 °C, revealing progressive color lightening and sintering intensification. At 800 °C, light gray loose powder indicates initial oxidation where ZrO<sub>2</sub>, amorphous B<sub>2</sub>O<sub>3</sub>, and SiO<sub>2</sub> form protective surface films without particle bonding. By 1000 °C, pure gray coloration and incipient sintering emerge as molten B<sub>2</sub>O<sub>3</sub>-SiO<sub>2</sub> eutectics enable liquidphase particle bridging. At 1200 °C, grayish-white coarsened agglomerates form through: (1) accelerated B<sub>2</sub>O<sub>3</sub> volatilization, (2) ZrO<sub>2</sub>/SiO<sub>2</sub> solid-state diffusion bonding, and (3) residual glassy phase pore-filling. At 1500 °C, further whitening accompanies consolidated agglomerates where SiO<sub>2</sub> fluidity enables particle rearrangement while ZrO<sub>2</sub> densifies, forming a rigid oxide skeleton after near-complete B<sub>2</sub>O<sub>3</sub> evaporation.

Fig. 6 presents scanning electron microscopy (SEM) images of SiC-ZrB<sub>2</sub> composite powders oxidized at 800 °C, 1000 °C, 1200 °C, and 1500 °C. At 800 °C, the oxidized product primarily revealed aggregated short rod-like, subspherical, and flake-shaped particles (Fig. 6a). When temperature increased to 1000 °C, short rod-like particles decreased markedly while subspherical and flake-like morphologies remained largely unaltered (Fig. 6b). At 1200 °C and 1500 °C, extensive particle coalescence occurred, forming densified agglomerates (Figs. 6c-d). These microstructural observations directly

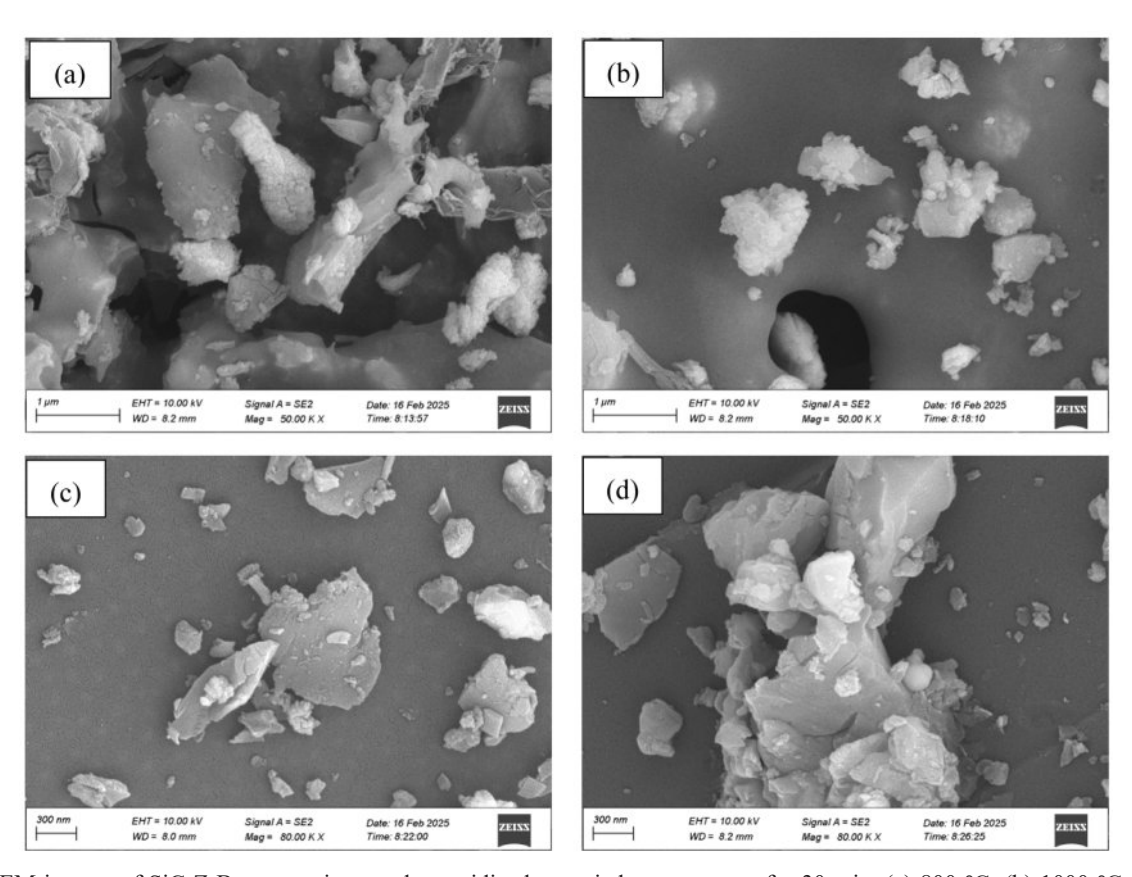


**Fig. 6.** SEM images of SiC-ZrB<sub>2</sub> composite powders oxidized at varied temperatures for 30 min. (a) 800 °C; (b) 1000 °C; (c) 1200 °C; (d) 1500 °C.

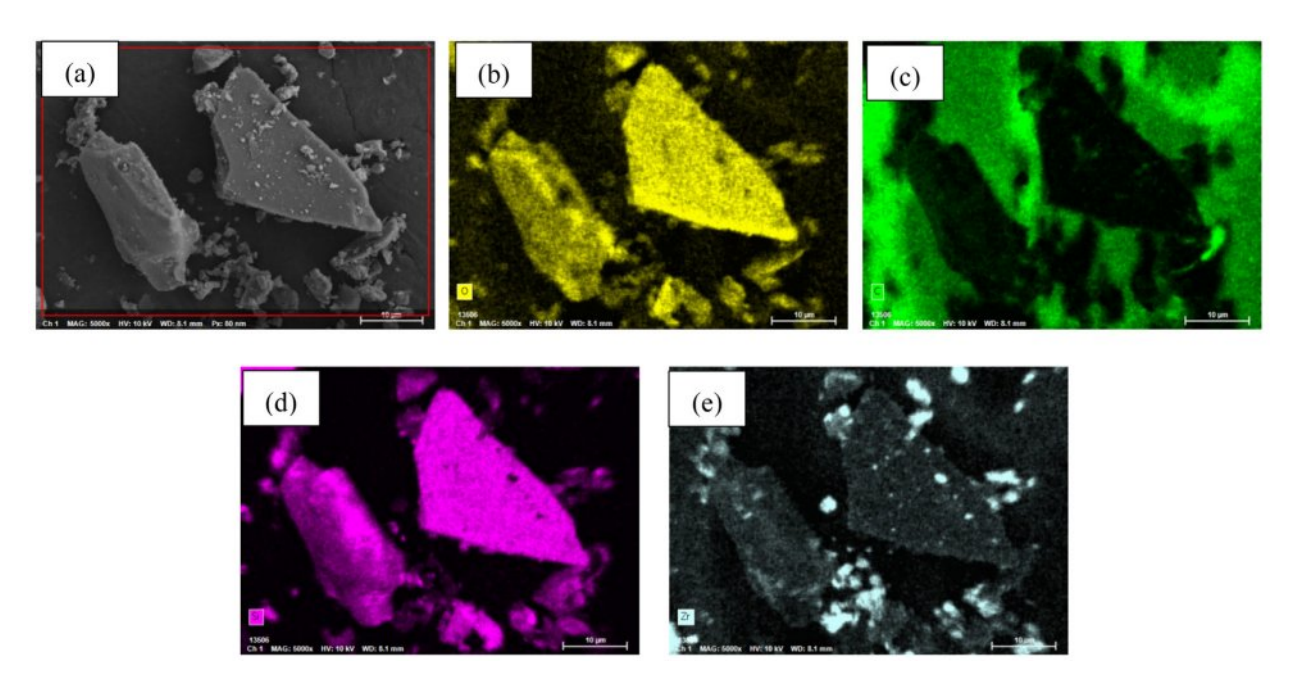


Fig. 7. EDX elemental mapping of SiC-ZrB<sub>2</sub> composite powders oxidized at 1000 °C for 30 min.

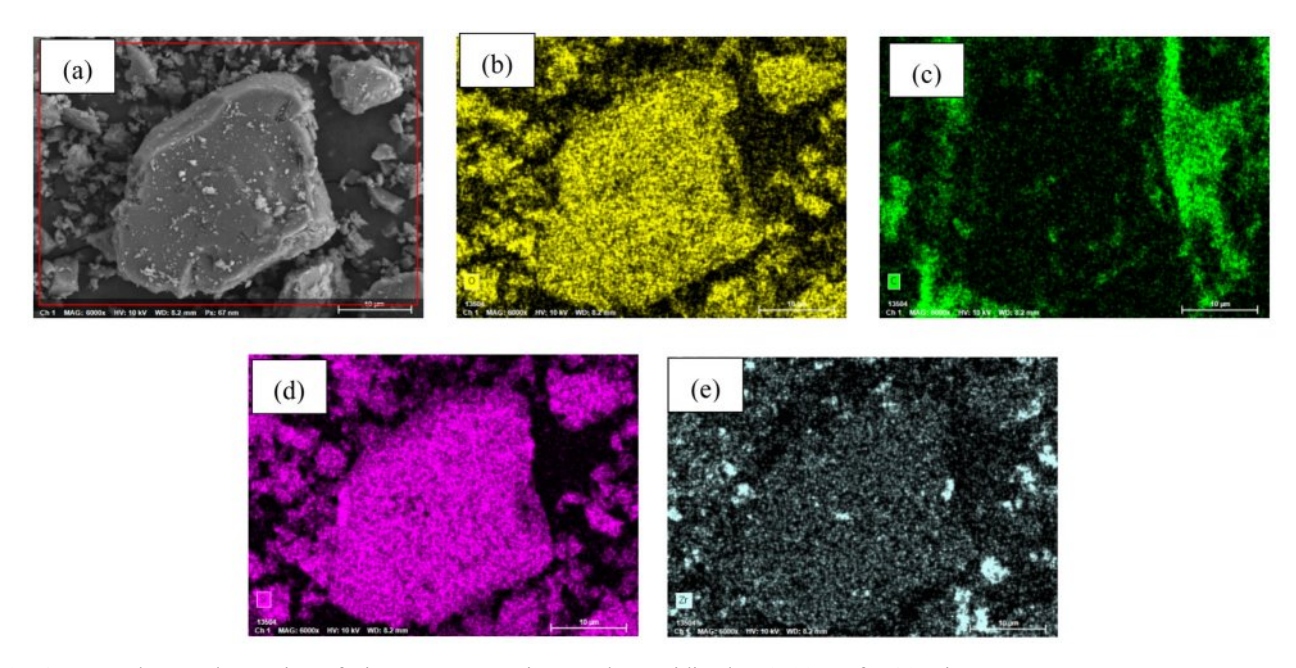


Fig. 8. EDX elemental mapping of SiC-ZrB<sub>2</sub> composite powders oxidized at 1500 °C for 30 min.

correlate with Fig. 5's macroscopic sintering progression, confirming temperature-dependent evolution across multiple length scales.

Figs. 7 and 8 present EDX elemental mapping of SiC-ZrB<sub>2</sub> composite powders oxidized at 1000 °C and 1500 °C, respectively. Table 3 quantifies elemental mass percentages from EDX mapping at these temperatures. Both samples contained carbon (C), oxygen (O), silicon (Si), and zirconium (Zr), but exhibited no detectable boron (B), confirming complete ZrB<sub>2</sub> oxidation to ZrO<sub>2</sub> and volatile B<sub>2</sub>O<sub>3</sub>. Comparative analysis reveals

**Table 3.** Elemental distribution (EDX mapping) for SiC-ZrB<sub>2</sub> powder after 30-min oxidation at 1000 °C and 1500 °C.

	С	О	Si	Zr	Total/%
1000 °C	21.83	28.12	38.68	11.38	100.00
1500 °C	6.37	42.20	41.07	10.36	100.00

significantly diminished carbon content at 1500 °C (Fig. 8b) versus 1000 °C (Fig. 7b), indicating intensified SiC oxidation at elevated temperatures. These EDX results

align with XRD phase analysis and SEM microstructural observations, demonstrating technique-consistent oxidation behavior.

#### Conclusion

During carbothermal reduction synthesis under argon protection, calcination temperature governed the phase composition of SiC-ZrB<sub>2</sub> composite powders. At 1450 °C, the product contained residual carbon, intermediate ZrSiO<sub>4</sub>, and minor ZrB<sub>2</sub>, indicating concurrent reactions where ZrO<sub>2</sub> partially formed zircon with SiO<sub>2</sub> while partially reducing to ZrB<sub>2</sub> with carbon. Increasing temperature to 1550 °C eliminated ZrSiO<sub>4</sub> through decomposition, initiated SiC formation via carbothermal reduction, and increased ZrB<sub>2</sub> content. After 1 h at 1600 °C, the reaction completed, yielding phase-pure SiC-ZrB<sub>2</sub> composite powders exhibiting a heterogeneous microstructure comprising quasi-spherical particles (50–150 nm), columnar particles, irregular aggregates, and abundant whisker-like SiC structures (~50-100 nm diameter).

Oxidation behavior analysis revealed temperature-dependent transitions: At 800 °C, ZrB<sub>2</sub> fully oxidized to ZrO<sub>2</sub> while partial SiC oxidation yielded ZrSiO<sub>4</sub>. By 1000 °C, increased ZrO<sub>2</sub> content and progressive SiC oxidation occurred alongside incipient powder sintering. Above 1200 °C, intensified SiC oxidation and accelerated sintering formed hardened agglomerates. Notably, at 1500 °C, SiC maintained structural stability-demonstrating significantly superior oxidation resistance compared to ZrB<sub>2</sub> under equivalent conditions.

#### Acknowledgements

This research was supported by the National Natural Science Foundation of China (Grant No. 52032011), and the Natural Science Foundation of Hunan Province, China (Grant No. 2025JJ70346).

#### References

- F. Zhan, R. Bai, X. Liu, K. Xu, H. Zhang, M. Zhu, Y. Zheng, S. Xu, J. Sheng, and P. La, J. Ceram. Process. Res. 25[4] (2024) 490-498.
- R. Hassan, W.G. Fahrenholtz, K. Balani, G.E. Hilmas, and J. Watts, Ceram. Int. 50[24PC] (2024) 55650-55657.
- M. Yang, B. Park, Y. Park, I. Oh, and H. Park, J. Ceram. Process. Res. 26[1] (2025) 51-57.
- X.H. Zuo, Z.J. Dong, G.M. Yuan, Z.W. Cui, and X.K. Li, J. Ceram. Process. Res. 22[1] (2021) 31-38.
- 5. X. Li, J. Feng, G. Zhao, and X. Wu, J. Ceram. Process.

- Res. 24[5] (2023) 816-826.
- C. Jiang, X. Ji, Y. Chen, P. Wang, P.V.K. Korneev, E.A. Levashov, J. Shi, X. Ren, X. Kang, B. Zhang, P. Zhang, L. Xu, and P. Feng, J. Eur. Ceram. Soc. 45[9] (2025) 117293
- 7. J.S. Choi, J.H. Kim, J.U. Hur, S.C. Choi, and G.S. An, J. Ceram. Process. Res. 21[3] (2020) 351-357.
- K. Gürcan, B. Yılmaz, and E. Ayas, J. Ceram. Process. Res. 18[4] (2017) 280-284.
- J.H. Leea, B.S. Jina, M.K. Kanga, I.Y. Kimb, A.G. Jeonc, J.H. Parka, D.K. Kimd, and Y.D. Shina, J. Ceram. Process. Res. 14[4] (2013) 577-582.
- L. Liu, C. Wei, W. Ou, F. Meng, S. Li, X. Duan, D. Chen, and H. Wang, J. Eur. Ceram. Soc. 44[4] (2024) 1898-1907.
- R. Bai, F. Zhan, H. Zhang, M. Zhu, Y. Zheng, and P. La,
  J. Ceram. Process. Res. 26[2] (2025) 219-230.
- B. Xie, L. Ma, X. Lin, Y. Liu, Y. Zhang, H. Gong, and W. Zhang, Ceram. Int. 44[16] (2018) 19522-19525.
- 13. Z. Zhou, D. Xia, Z. Li, H. Liao, and X. Jin, Mater. Sci. Eng. Powder Metall. 28[3] (2023) 223-232.
- X. Lian, X. Hua, X. Wang, and L. Deng, Mater. 13[16] (2020) 3502.
- Y. Cao, H. Zhang, F. Li, L. Lu, and S. Zhang, Ceram. Int. 41[6] (2015) 7823-7829.
- T. Wang, Y. Zhang, J. Li, B. Zhao, R. Li, S. Yin, Z. Feng, T. Sato, and H. Cai, J. Nanosci. Nanotechnol. 15[9] (2015) 7402-7406.
- 17. W.W. Wu, G.J. Zhang, Y.M. Kan, and P.L. Wang, Mater. Lett. 63[16] (2009) 1422-1424.
- S. Sun, Y. Liu, Z. Ma, S. Zhu, and K. Ma, Powder Technol. 372 (2020) 506-518.
- Y. Zeng, J. Liu, F. Liang, H. Xu, H. Zhang, and S. Zhang,
  J. Am. Ceram. Soc. 102[5] (2018) 2426-2439.
- X. Deng, S. Du, H. Zhang, F. Li, J. Wang, W. Zhao, F. Liang, Z. Huang, and S. Zhang, Ceram. Int. 41[10] (2015) 14419-14426.
- S. Mun, K.H. Kim, S. Park, E. Kwon, M. Yang, H.S. Ahn, I. Jeon, H. Jeon, J.H. Lee, K. Jung, W.J. Lee, M.C. Shin, and S.M. Koo, J. Ceram. Process. Res. 26[1] (2025) 82-90.
- S. Dhage, H.C. Lee, M.S. Hassan, M.S. Akhtar, C.Y. Kim, J.M. Sohn, K.J. Kim, H.S. Shin, and O.B. Yang, Mater. Lett. 63[2] (2009) 174-176.
- Y. Peng, Z. Meng, C. Zhong, J. Lu, W. Yu, and Y. Qian, Mater. Res. Bull. 36[9] (2001) 1659-1663.
- X. Xing, J. Chen, G. Bei, B. Li, K.C. Chou, and X. Hou, J. Adv. Ceram. 6[4] (2017) 351-359.
- J. Wang, S. Du, X. Deng, H. Zhang, and S. Zhang, J. Chin. Ceram. Soc. 43[9] (2015) 1197-1202.
- Y. Fang, Z. Zhang, Y. Wang, J. Peng, H. Zhang, and J. Liu, Rare Met. Mater. Eng. 53[11] (2024) 3259-3270.
- J. Liu, L. Xu, W. Yue, M. Zhang, X. Li, S. Wang, Q. Liu,
  C. Ma, H. Yuan, and J. Cui, Ceram. Int. 50[20PA] (2024) 38200-38208.
- Z. Hong, Q. Zhang, K. Li, H. Guo, C. Zhang, and Y. Liu,
  J. Mater. Eng. 49[5] (2021) 144-150.